Journal of Power Sources 270 (2014) 292–303

Contents lists available at ScienceDirect

Journal of Power Sources

journal homepage: www.elsevier.com/locate/jpowsour

Enhanced proton conductivity of the hybrid membranes by regulating the proton conducting groups anchored on the mesoporous silica

Yuning Zhao [a, b], Hao Yang [a, b], Hong Wu [a, b, c], Zhongyi Jiang [a, b, *]

[a] Key Laboratory for Green Chemical Technology, Ministry of Education of China, School of Chemical Engineering and Technology, Tianjin University, Tianjin 300072, China
[b] Collaborative Innovation Center of Chemical Science and Engineering (Tianjin), Tianjin 300072, China
[c] Tianjin Key Laboratory of Membrane Science and Desalination Technology, Tianjin University, Tianjin 300072, China

HIGHLIGHTS

- The outer surfaces of mesoporous silica were modified by $-NH_2$ or $-PO_3H_2$ groups.
- The inner pore walls of mesoporous silica were modified by $-PO_3H_2$ groups.
- Hybrid membrane was made by adding differently modified SiO_2 into Nafion matrix.
- Proton conductivities of hybrid membranes were all enhanced.
- Hybrid membranes had different proton conduction behavior under low humidity.

GRAPHICAL ABSTRACT

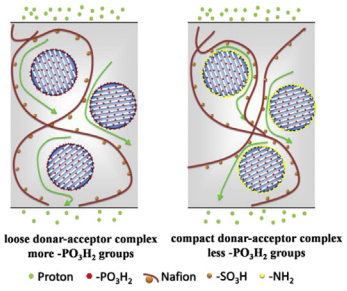

ARTICLE INFO

Article history:
Received 31 May 2014
Received in revised form
19 July 2014
Accepted 21 July 2014
Available online 27 July 2014

Keywords:
Mesoporous silica submicrospheres
Amination
Phosphorylation
Nafion
Hybrid
Proton exchange membrane

ABSTRACT

Mesoporous silica submicrospheres with $-NH_2$ groups or $-PO_3H_2$ groups on the outer surface, and $-PO_3H_2$ groups on the inner pore walls are prepared and designated as N–P–SiO_2 and P–P–SiO_2, respectively. Both kinds of silica submicrospheres are introduced into Nafion membrane matrix to fabricate hybrid membranes. The water uptake, membrane swelling properties, and proton conductivities at different temperatures and different relative humidities of the hybrid membranes are characterized. Proton conducting performances of the hybrid membranes are all enhanced compared to that of the pristine Nafion membrane, and the highest proton conductivity is 0.339 S cm^{-1} (115 °C, 100% RH). At 100% RH, Nafion/N–P–SiO_2 membranes exhibit higher proton conductivities than the Nafion/P–P–SiO_2 counterparts; while at low humidities, the proton conductivities of the Nafion/P–P–SiO_2 membranes are enhanced more pronouncedly than those of the Nafion/N–P–SiO_2 counterparts. The different increasing tendencies of the proton conducting performance could be attributed to the varied synergistic effects between the proton conducting groups introduced by the mesoporous silica and the groups anchored on the membrane matrix.

1. Introduction

Proton exchange membrane fuel cells (PEMFC) have become competitive energy conversion devices for the advantages of fast start, high power density and efficiency, and no emission of

* Corresponding author. Key Laboratory for Green Chemical Technology, Ministry of Education of China, School of Chemical Engineering and Technology, Tianjin University, Tianjin 300072, China. Tel./fax: +86 022 23500086.
E-mail address: zhyjiang@tju.edu.cn (Z. Jiang).

http://dx.doi.org/10.1016/j.jpowsour.2014.07.135
0378-7753/

pollutants; and nowadays, some commercialized PEMFCs have already been available around the world [1,2]. High-performance proton exchange membrane (PEM) is vital for the fabrication of practical fuel cells, and a variety of proton conducting groups have been employed to enhance the proton conducting property of PEMs.

Proton conducting process exists, not only in electrochemical energy conversion process, but also in nature, such as biological systems [1]. The most efficient proton conducting carrier in nature is "proton pump": in which proton is conducted along the "proton wires" formed by the amino acid residues [3]. The transport proteins of bacteriorhodopsin are typical kinds of proton pump, which are composed of seven α-helical membrane proteins, and the chromophores are bonded by Schiff base [4]. By photoinitiation, different kinds of metastable protein isoforms are generated along with the protonation and deprotonation of the Schiff base, hence protons are transferred across the cell membranes. The fast proton conduction takes place between the amino acid residues, *i.e.* the synergistic effects between $-NH_2$ groups and $-COOH$ groups are beneficial to the successive breaking and forming of hydrogen bonds, and thus contribute to the proton conduction along the hydrogen networks.

Numerous kinds of hybrid membranes have been fabricated to enhance the membrane performance by firstly fixing proton conducting groups to the inorganic skeletons, and then introducing the modified inorganic fillers to the organic matrix [5–14]. The added proton conducting groups such as $-SO_3H$, $-PO_3H_2$ and imidazole groups could enhance proton conducting properties by rendering abundant proton conducting sites. Meanwhile, the synergistic effects between the proton conducting groups anchored on both the inorganic skeletons and the organic matrix also make some contributions to the promotion of proton conducting property. There are multiple kinds of synergistic interactions between the proton donating groups and the proton accepting groups [3,15–17]: (i) Tight proton donor–acceptor complexes: interactions (such as electrostatic attraction and ionic bonds) are formed in the complexes and the proton conducting groups in the complexes are hydrated as a whole. Fast proton conduction could be acquired along with the moderate rearrangement of the hydration shells. (ii) Loose proton donor–acceptor complexes: the proton conducting groups are hydrated separately and connected by water molecules in between. If there are less than four water molecules as the connecting groups, water molecules could arrange in favorable orientations for proton conduction, and fast proton conduction could also be facilitated by the complexes. (iii) If the proton donating groups and proton accepting groups are isolated by more water molecules, both kinds of groups are hydrated separately. Thus the proton conduction would be accompanied by the rearrangement of the hydration shells of each group, together with the diffusion of protons among the water molecules isolating the proton conducting groups. As a result, the transportation of protons would be obviously limited. Herein, by regulating the proton conducting groups on the inorganic skeletons could adjust the synergistic interactions in between the proton conducting groups especially in the organic–inorganic interface zone of the hybrid membranes, and facilitate proton conduction.

In this study, mesoporous silica submicrospheres (SiO_2) with different kinds of proton conducting groups on the outer surfaces were prepared and incorporated into Nafion matrix to form hybrid membranes. The outer surface and the inner pore walls of SiO_2 could be modified by different kinds of groups through tuning the modification methods. $-NH_2$ groups were anchored on the outer surface of silica and the inner pore walls were phosphorylated ($N-P-SiO_2$); and alternatively, both the outer surface and the inner pore walls were phosphorylated ($P-P-SiO_2$). The water uptake, membrane swelling properties, and proton conductivities at different temperatures and different relative humidities of these two kinds of hybrid membranes have been characterized. Consequently, different kinds of synergistic interactions were investigated to exploit high-performance proton conducting membranes.

2. Experiment

2.1. Materials and chemicals

Tetraethyl orthosilicate (TEOS, 98%) was purchased from Sigma–Aldrich Co. LLC.; hexadecyltrimethyl ammonium bromide (CTAB, 99%), (3-aminopropyl)triethoxysilane (APTES, 99%) and 3-glycidyloxypropyltrimethoxysilane (GPTMS, 97%) were purchased from Aladdin Industrial Inc. Phosphorus oxychloride ($POCl_3$, >98 wt.%) and Nafion (DuPont D520, 5 wt.%) were purchased from Shanghai Guangzan Chemical Scientific Ltd. and Shanghai Hesen Electric Co., Ltd., respectively. Toluene (AR) was purchased from Tianjin Jiangtian Chemical Technology Co., Ltd. and was refined by distillation before use especially to eliminate the water molecules.

All the other materials and chemicals were commercially available and used without further purification. Deionized water was used in the experiment.

2.2. Preparation of different kinds of modified mesoporous silica submicrospheres

2.2.1. Preparation of mesoporous silica submicrospheres modified by both $-NH_2$ and $-PO_3H_2$ groups ($N-P-SiO_2$)

Mesoporous silica submicrospheres were prepared by the typical procedure for the synthesis of MCM-41 as reported in our previous work with little modification [18]: both CTAB (0.8 g) and NaOH aqueous solution (3.5 mL, 2 M) were dissolved in 480 mL of water and the solution was kept stirring at 80 °C for 40 min. Then, 5 mL of TEOS was added and the reaction was carried on at 80 °C for 3 h more with constant stirring. Afterward, mesoporous silica submicrospheres with CTAB as templates ($CTAB-SiO_2$) were obtained and purified by three cycles of centrifugation and redispersed in ethanol (ethanol purification), and dried in a vacuum oven at room temperature till constant weight.

To anchor the $-NH_2$ groups only on the outer surface of the mesoporous silica submicrospheres, $CTAB-SiO_2$ was used to react with APTES in the refined toluene according to the procedure in our previous work [19]. Then, the $-NH_2$ groups modified $CTAB-SiO_2$ was refluxed in solution of hydrochloric acid in methanol to remove the template CTAB by the method in our previous work with little modification [18]: 1.5 g of silica was refluxed in solution of hydrochloric acid (9 mL) in methanol (160 mL) at 65 °C for 48 h. Afterward, $-NH_2$ groups modified silica ($N-SiO_2$) was obtained and purified by ethanol purification, and dried in a vacuum oven at room temperature till constant weight.

Subsequently, the inner mesopore walls of $N-SiO_2$ were phosphorylated by the reaction of $POCl_3$ and the epoxy groups introduced by GPTMS according to the method in our previous work [19]. The obtained mesoporous silica submicrospheres with $-NH_2$ groups on the outer surface and $-PO_3H_2$ groups on the inner pore walls ($N-P-SiO_2$) were purified by ethanol and dried in a vacuum oven at room temperature till constant weight.

2.2.2. Preparation of mesoporous silica submicrospheres modified by $-PO_3H_2$ groups ($P-P-SiO_2$)

Mesoporous silica submicrospheres with $-PO_3H_2$ groups both on the outer surface and inner pore walls ($P-P-SiO_2$) were prepared in the same way with $N-P-SiO_2$. Firstly, $CTAB-SiO_2$ was phosphorylated by the reaction of $POCl_3$ and the epoxy groups

introduced by GPTMS according to the method in our previous work [19]. Secondly, CTAB template was removed by reflux in the solution of hydrochloric acid in methanol [18]. Thirdly, the inner pore walls were phosphorylated and the obtained P–P–SiO_2 was dried in a vacuum oven at room temperature till constant weight.

Mesoporous silica submicrospheres (SiO_2) were prepared by directly removing the CTAB template of CTAB–SiO_2. The preparation process for SiO_2, N–P–SiO_2 and P–P–SiO_2 was depicted in Scheme 1.

2.3. Membrane preparation

Both the pristine and the hybrid Nafion membranes were fabricated by recast of Nafion® solution [20]. Firstly, the purchased Nafion® solution (5 wt.%) was dried at 60 °C till constant weight to evaporate the solvent. Secondly, the transparent resinous Nafion (0.2 g) was dissolved in dimethylacetamide (DMAC, 1 g); meanwhile, SiO_2 (or N–P–SiO_2, P–P–SiO_2; the weight percent of which relative to the dried Nafion was Z wt.%) was well dispersed in DMAC (1 g). Thirdly, the solutions of both Nafion and inorganic fillers were finely mixed together, and then casted onto clean glass plate. The membrane was dried at 80 °C for 12 h, followed by further heat treatment at 120 °C for another 12 h. The pristine Nafion membrane was fabricated by directly casting of DMAC solution of Nafion without inorganic additives.

The obtained membranes were purified firstly to remove the organic residues from the purchased Nafion® solution before use, and the entire treatment was kept at 80 °C. The membranes were heated in H_2O_2 solution (3 wt.%) for 30 min to oxidize the organic residues, and subsequently heated in water for 30 min to eliminate H_2O_2. Next, the membranes were treated in H_2SO_4 solution (1 M) for 30 min to ion-exchange the proton conducting groups into acidic form, and then washed by deionized water to eliminate the residual H_2SO_4 till the neutral pH was reached. The final membranes were dried in a vacuum oven at room temperature till constant weight. It's accepted that by treating Nafion membrane in H_2O_2 solution, the proton conducting channels of Nafion are more broadened and better connected [21]. The hybrid membranes containing N–P–SiO_2 (or P–P–SiO_2, SiO_2) were denoted as Nafion/N–P–SiO_2–Z (or Nafion/P–P–SiO_2–Z, Nafion/SiO_2–Z), where Z referred to the weight percentage (Z wt.%). The thickness of both the pristine and hybrid membranes was about 30 μm.

2.4. Characterization

The size, morphology and the meso-structure of both the pristine silica and the modified submicrospheres were observed by high resolution transmission electron microscopy (HRTEM-Tecnai G2 F20, FEI). The cross-sectional morphology of the membranes and the dispersity of inorganic fillers were observed by field emission scanning electron microscope (FESEM, Nanosem 430, FEI). The Brunauer–Emmett–Teller (BET) specific surface area of the synthesized mesoporous silica submicrospheres was determined by measuring nitrogen adsorption/desorption isotherm (TriStar 3000), and the pore size, pore volume were calculated using the Barrett–Joyner–Halenda (BJH) formula [22].

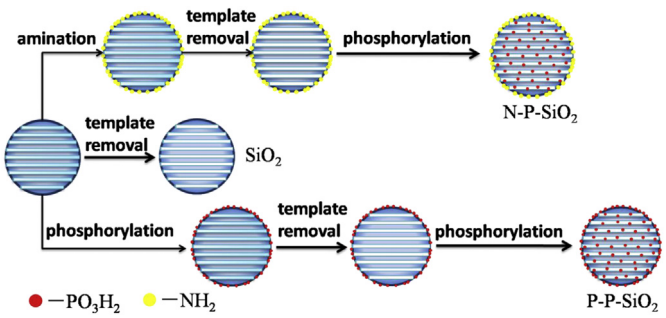

Scheme 1. Schematic depiction of the preparation process of the modified mesoporous silica submicrospheres.

The phosphorus contents and the nitrogen content of N–P–SiO_2 and P–P–SiO_2 submicrospheres were analyzed by inductively coupled plasma optical emission spectrophotometer (ICP, ICP-9000 (N + M), USA Thermo Jarrell-Ash Corp.) and elemental analyzer (Vairo EL, Elementar), respectively. The surface elemental valence states of P and N of the modified submicrospheres were analyzed by X-ray photoelectron spectroscopy (XPS, Axis Ultra DLD, Kratos Analytical Ltd.) with a Mg/Al radiation for excitation.

The thermal stabilities of both the silica submicrospheres and the membranes were analyzed by thermogravimetric analyzer (TG 209 F3, Proteus Thermal Analysis, NETZSCH) from room temperature to 800 °C at a heating rate of 10 °C min^{-1} in nitrogen atmosphere with the flow rate of 30 mL min^{-1}. The glass transition process of the membranes was recorded by differential scanning calorimetry (DSC 200F3, NETZSCH) in N_2 flow. Firstly, the membrane samples were heated from room temperature to 100 °C at a heating rate of 10 °C min^{-1}, then kept at100 °C for 4 min, thus the residual water molecules were evaporated. Secondly, the samples were cooled to 60 °C at a cooling rate of 60 °C min^{-1} to eliminate the effect of crystallization process. Finally, the glass transition process was recorded from 60 °C to 200 °C at a heating rate of 10 °C min^{-1}.

2.5. Water uptake and swelling properties

The dry membrane samples were cut into rectangle shape (about 1 × 4 cm), and the water uptake and swelling properties were calculated based on the weight or volume increments of the samples after fully hydration of the dry samples, respectively. According to the method in the previous work, the water uptake and swelling were calculated by Equations (1) and (2) [23]:

$$\text{water uptake}(\%) = \left(W_{wet} - W_{dry}\right) \Big/ W_{dry} \times 100 \quad (1)$$

$$\text{swelling}(\%) = \left(V_{wet} - V_{dry}\right) \Big/ V_{dry} \times 100 \quad (2)$$

where W_{dry} and V_{dry} were the weight (g) and volume (cm^3) of the dry membranes, W_{wet} and V_{wet} were the weight (g) and volume (cm^3) of the fully hydrated membranes, respectively. The measurements were repeated three times, and the error was within ±5%.

2.6. Proton conducting property

2.6.1. Proton conductivity at 100% RH with rising temperature

The in-plane proton conductivities of the membranes were measured by a two-point-probe conductivity cell with the relative humidity kept at 100% and the testing membrane temperature increasing from room temperature to 130 °C according to the method in the previous work [23]. The two-point-probe conductivity cell was placed in a sealed stainless steel container with polytetrafluoroethylene liner. Deionized water was utilized in the container and heated to maintain the temperature and relative humidity. Pressure and temperature were detected by piezometer and thermoelement, respectively. And the proton conducting data were collected by AC impedance spectroscopy (Autolab PGSTST20,

The Netherlands) using a frequency response analyzer (Parstat2273 Advanced Electrochemical System, FRA, Compactstat, IVIUM Tech.) over a frequency range of 1–10^6 Hz with an oscillating voltage of 20 mV. The membrane samples were fully hydrated by water before the measurements. The proton conductivity σ (S cm^{-1}) was calculated by the following equation (Equation (3)):

$$\sigma = l/(A \times R) \quad (3)$$

where l was the distance between the two electrodes (cm); A was the effective cross-sectional area of the testing membrane (cm^2); R was the measured resistance (Ω).

2.6.2. Proton conductivity at 80 °C and low humidity

The in-plane proton conductivities of the membranes at 80 °C and low humidity were measured by the same device described in Section 2.6.1. The low humidities were maintained by using different kinds of salt solutions instead of water in the conductivity cell. The saturated steam of K_2CO_3, $NaNO_2$ and KBr saturated solutions could provide the tested membranes with the relative humidity of 41%, 57% and 78% at 80 °C, and the proton conductivity was also calculated according to the Equation (3).

3. Results and discussions

3.1. Characterizations of mesoporous silica submicrospheres

By controlling the synthesis processes, *i.e.* the sequence of removing of the mesoporous template (CTAB) and the modification by either $-NH_2$ or $-PO_3H_2$ groups, the outer surface and the inner pore walls of the mesoporous silica could be modified by different kinds of functional groups, thus realizing the preparation of both N–P–SiO_2 and P–P–SiO_2 submicrospheres. The morphology and size of the mesoporous silica submicrospheres were observed by TEM and shown in Fig. 1. It could be observed that SiO_2 exhibited uniform spherical morphologies with the diameter of about 100 nm (Fig. 1(a)). Furthermore, the regular morphologies were kept intact after modification by either $-NH_2$ or $-PO_3H_2$ groups (Fig. 1(b) and Fig. 1(c) for P–P–SiO_2 and N–P–SiO_2, respectively). The meso-structure of the mesoporous silica submicrospheres was further observed and shown in Fig. 2. It could be clearly observed that both SiO_2 and the modified submicrospheres exhibited one-dimensional hexahedral mesopores regularly arranged in parallel. The integrity of the meso-structures of mesoporous silica submicrospheres after different modifications was proved. The successful preparation of different kinds of mesoporous silica submicrospheres was confirmed.

The meso-structures of the synthesized mesoporous silica submicrospheres were determined quantitatively by BET method and calculated according to the BJH formula (the detailed structural parameters were listed in Table 1). The specific surface area, pore size and pore volume of SiO_2 were 906.1 m^2 g^{-1}, 10.4 nm and 0.858 cm^3 g^{-1}, respectively. All the meso-structural parameters of silica were reduced after the modification by either $-NH_2$ or $-PO_3H_2$ groups, and the pore sizes were in the range of 7.6–7.7 nm, which could also suggest the successful anchorage of proton conducting groups on the outer surface and the inner pore walls.

The chemical structures of the mesoporous silica submicrospheres were characterized by ICP, elemental analyzer and XPS; the elemental contents were listed in Table 1, and the XPS spectra were shown in Fig. 3. The contents of P element on the outer surface only or on the inner pore walls only of P–P–SiO_2 were 2.31 and 1.41, respectively; the content of N element on the outer surface only and that of P element on the inner pore walls only of N–P–SiO_2 were 1.69 and 1.73, respectively. It was shown that the content of P element on the inner pore walls only of N–P–SiO_2 was higher than that of P–P–SiO_2 (increased by 22.7%). It was clarified that both P–P–SiO_2 and N–P–SiO_2 were modified for the outer surface only first, and then phosphorylated for the inner pore walls. As a result, the inner pore walls of both P–P–SiO_2 and N–P–SiO_2 were phosphorylated with the outer surface already functionalized by either $-PO_3H_2$ or $-NH_2$ groups. It was accepted that the ring–opening reaction of epoxy groups could be accelerated under basic conditions [24], therefore the phosphorylation of the inner pore walls of N–P–SiO_2 could be facilitated with the existence of $-NH_2$ groups, resulting in the higher P content of N–P–SiO_2. The oxidation states of P or N elements of both P–P–SiO_2 and N–P–SiO_2 were analyzed by XPS, and the peak values of the bond energy of both P and N elements were around 134 eV and 400 eV, respectively. Accordingly, it was proved that P elements of both P–P–SiO_2 and N–P–SiO_2 were in the pentavalent states and existed in the form of P–O bonds; besides, the N element of N–P–SiO_2 was in the form of $-NH_2$ groups. The chemical structures of the mesoporous silica submicrospheres were depicted in Scheme 1.

3.2. Characterizations of the hybrid membranes

The prepared mesoporous silica submicrospheres were incorporated into Nafion matrix to fabricate Nafion hybrid membranes. The cross-sectional morphology of the membranes and the dispersity of the inorganic fillers were observed by FESEM (Fig. 4). It

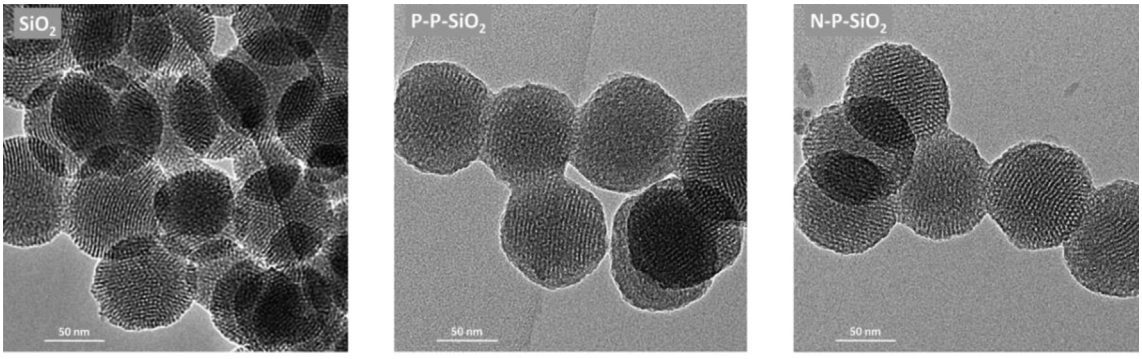

Fig. 1. HRTEM images of the (a) SiO_2, (b) P–P–SiO_2 and (c) N–P–SiO_2 submicrospheres.

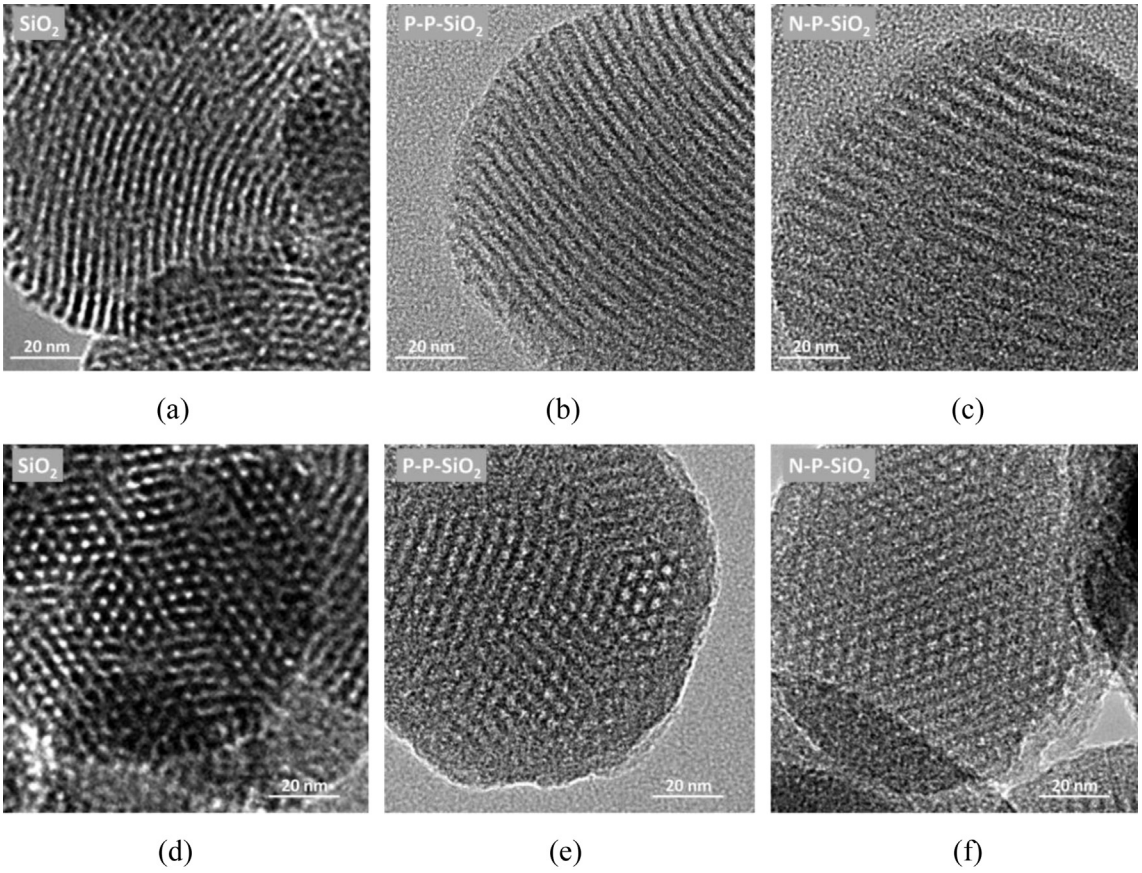

Fig. 2. HRTEM images of the meso-structures of (a) SiO_2, (b) P–P–SiO_2 and (c) N–P–SiO_2 submicrospheres observed in the direction of perpendicular to the mesopores; and HRTEM images of the meso-structures of the (d) SiO_2, (e) P–P–SiO_2 and (f) N–P–SiO_2 submicrospheres observed in the direction of parallel to the mesopores.

was shown that the recast pristine Nafion membrane was homogeneous and dense (Fig. 4(a)), meanwhile, the organic matrix of all the hybrid membranes were consistent with the pristine Nafion membrane. With the content of 5 wt.%, the inorganic fillers were homogeneously dispersed in the hybrid membranes, suggesting the fine compatibility of the inorganic fillers and the organic matrix (Fig. 4(b), (d) and (f) for Nafion/P–P–SiO_2–5, Nafion/N–P–SiO_2–5 and Nafion/SiO_2–5, respectively). Minor aggregation of the inorganic fillers was observed with the content of 11 wt.% for all the hybrid membranes, whereas the inorganic fillers were still well dispersed.

Table 1
Structural parameters of the SiO_2, P–P–SiO_2 and N–P–SiO_2 submicrospheres.

Sample	Specific Surface area S_{BET} ($m^2\ g^{-1}$)	Pore size[a] (nm)	Pore volume[b] ($cm^3\ g^{-1}$)	Content of P element[c] (wt.%)	Content of N element[d] (wt.%)
SiO_2	906.1	10.4	0.858	0	0
P–P–SiO_2	355.0	7.7	0.156	Outer surface only[e]: 2.31 The entire content: 3.72 (inner pore walls only[f]: 1.41)	0
N–P–SiO_2	325.4	7.6	0.174	inner pore walls only: 1.73	outer surface only: 1.69

[a] Calculated from the BJH desorption branch of the isotherms.
[b] BJH desorption cumulative volume of pores.
[c] Obtained from ICP results.
[d] Obtained from element analyzer results.
[e] After the CTAB template removal of the phosphorylated CTAB–SiO_2, the submicrospheres were characterized by ICP to determine the content of P of the outer surface only.
[f] Calculated from the ICP results of the P content of the outer surface only and that of the entire P–P–SiO_2 submicrospheres.

The enthalpy change processes of both the pristine and the hybrid Nafion membranes were recorded by DSC and the glass transition temperatures (T_gs) were shown in Fig. 5. The T_g of the recast Nafion membrane was 105 °C, consistent with the reported data [25,26]. After the introduction of inorganic fillers into the membrane matrix, T_gs of the hybrid membranes were increased, suggesting the mobility decrease of the polymer matrix and the restriction of the polymer arrays. It is accepted that, polymer matrix would compact around the incorporated mesoporous fillers, and the polymer chains would pack tightly nearby the mesopores or even "block" the pores [27–29], thereby the T_gs of the Nafion/SiO_2 hybrid membranes were increased to about 111 °C. However, considering the different functional groups on the outer surfaces of N–P–SiO_2 and P–P–SiO_2, the interactions of the inorganic fillers and the organic matrix would be different from each other. There were electrostatic attractions or even electrostatic crossing-linking between the $-NH_2$ groups on the outer surface of N–P–SiO_2 and the $-SO_3H$ groups of Nafion matrix in the organic–inorganic interface zone, forming tight complexes of the proton accepting groups ($-NH_2$ groups) and the proton donating groups ($-SO_3H$ groups), hence generating interfacial stress in the interface region and further restricting the mobility of the polymer matrix. Thus the T_gs of the Nafion/N–P–SiO_2 hybrid membranes were increased to around 115 °C, higher than all the other hybrid membranes. The $-PO_3H_2$ groups are weak acidic groups, and can generate excess protons other than combining with the dissociated protons.

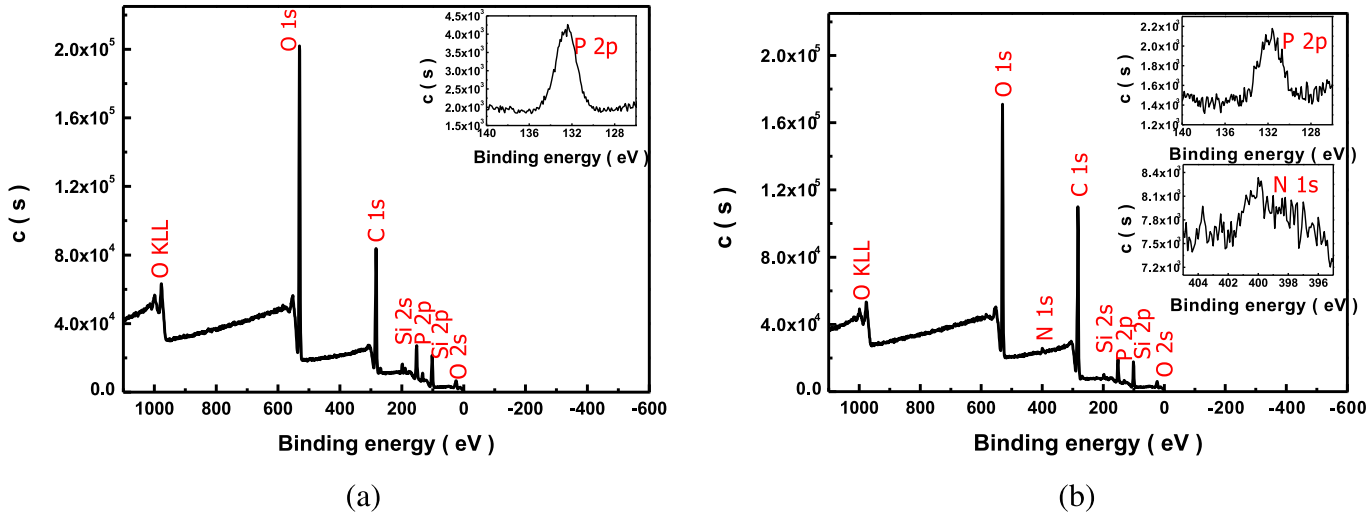

Fig. 3. XPS spectra of the (a) P–P–SiO_2 and (b) N–P–SiO_2 submicrospheres.

Therefore, besides forming hydrogen bonds between the $-PO_3H_2$ groups of P–P–SiO_2 and the $-SO_3H$ groups of Nafion matrix, and transferring of the dissociated protons from the $-SO_3H$ groups to the $-PO_3H_2$ groups, electrostatic repulsion could exist between these groups, and weaker proton acceptor–donator interactions were formed [19,30,31]. As a result, the tight packing of the polymer matrix nearby the mesopores of P–P–SiO_2 could be disturbed to a certain degree. Therefore the T_gs of the Nafion/P–P–SiO_2 hybrid membranes were increased to around 107 °C, lower than all the other hybrid membranes. Based on the above discussions, the interactions between the proton conducting groups in the hybrid interface could be deduced.

The thermal stabilities of the membranes were characterized by TGA and shown in Fig. 6. Both the pristine and the hybrid Nafion membranes exhibited the same type of degradation behavior, indicating that the thermal stabilities were not changed after the incorporation of the inorganic fillers. Firstly, the weight loss below ~200 °C was caused by the evaporation of the residual bound water in the membranes. And the degradation of all the membranes was in three steps: (i) the weight loss below ~340 °C was attributed to the decomposition of the $-SO_3H$ groups of Nafion matrix; (ii) the weight loss from 340 °C to ~380 °C was due to the decomposition of the polar perfluorinated sulfonic acid vinyl ether segments ($-CF_2-CF_2-O-CF_2-$); (iii) the weight loss from ~430 °C to ~520 °C was the further degradation of the membrane matrix, *i.e.* the decomposition of the non-polar perfluorovinyl segment ($-CF_2-CF_2-$) [26].

3.3. Water uptake and swelling properties of the hybrid membranes

The water uptake and swelling properties of all the membranes at 25 °C were shown in Fig. 7, and were 24.62% and 37.10% for the

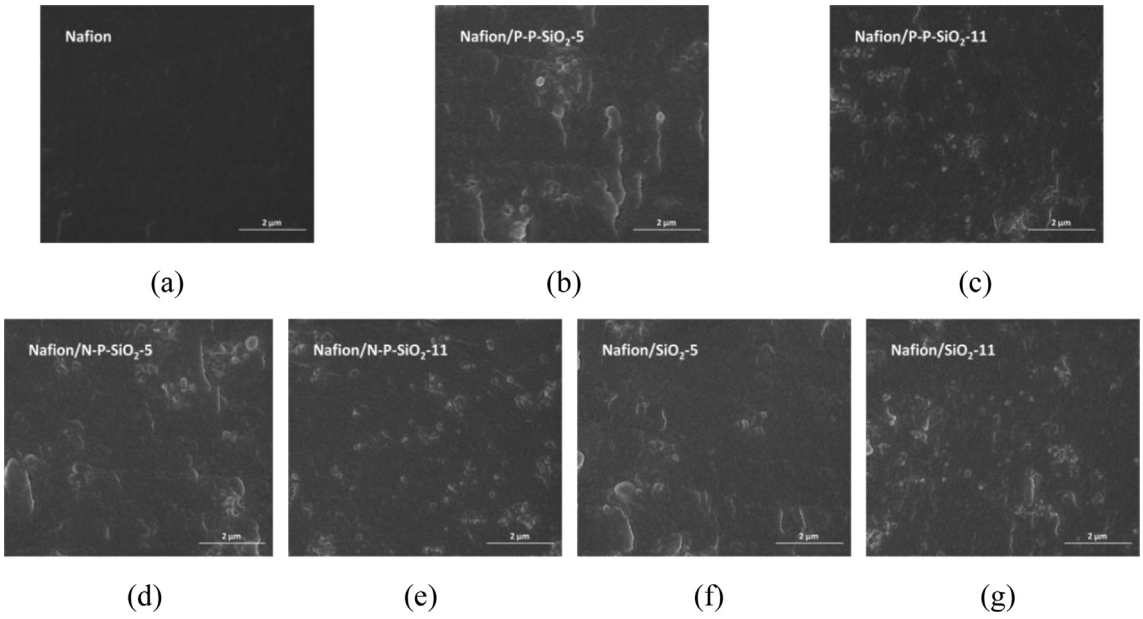

Fig. 4. FESEM images of the cross-section of the (a) pristine Nafion, (b) Nafion/P–P–SiO_2–5, (c) Nafion/P–P–SiO_2–11, (d) Nafion/N–P–SiO_2–5, (e) Nafion/N–P–SiO_2–11, (f) Nafion/SiO_2–5 and (g) Nafion/SiO_2–11 hybrid membranes.

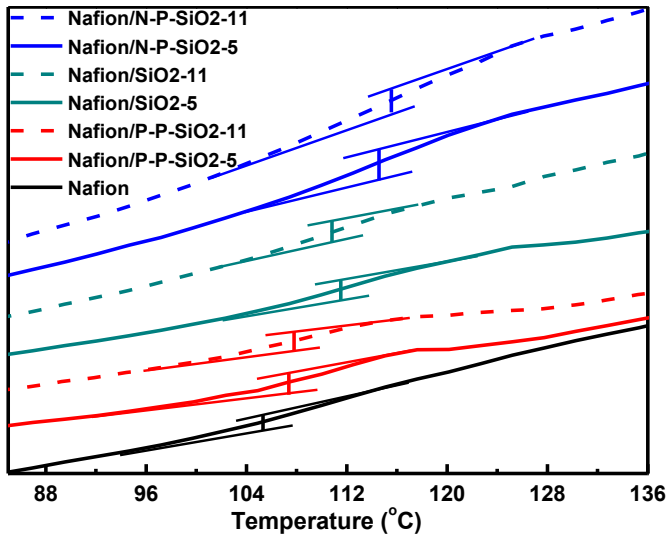

Fig. 5. DSC curves of the pristine and the hybrid Nafion membranes.

pristine Nafion membrane, respectively. Both the water uptake and swelling degrees were increased by the introduction of the inorganic fillers. The increasing rates of both the water uptake and swelling properties of the membranes were shown in Fig. 8. It could be observed that the dependence of water uptake and swelling on filler content had no big difference. Since the hygroscopic Si–OH groups on the silica surface and the mesopores of SiO_2 could absorb water by capillary forces, more water molecules could be contained in the Nafion/SiO_2 hybrid membranes. As a result, the water uptake and swelling degree were increased for the Nafion/SiO_2 hybrid membranes. The weaker proton acceptor–donator interactions between the $-PO_3H_2$ groups on the outer surface of P–P–SiO_2 and the $-SO_3H$ groups of Nafion matrix could limit the water uptake and swelling degree to some extent. Therefore, the water uptake and the swelling properties of the Nafion/P–P–SiO_2 hybrid membranes were in the same tendencies with the Nafion/SiO_2 membranes, but both values were lower than those of the Nafion/SiO_2 membranes. The tight electrostatic complexes formed by the $-NH_2$ groups on the outer surface of N–P–SiO_2 and the $-SO_3H$ groups of Nafion matrix in the organic–inorganic interface zone would further restrict the mobility of the polymer chains, and also decrease the water-bonding ability of the $-SO_3H$ groups. Although the water uptake and the swelling degree of the Nafion/N–P–SiO_2 membranes were higher than those of the pristine Nafion membrane, they were both in the decreasing tendency with the increasing inorganic content, and the decreasing tendency was more obvious for the swelling degrees.

3.4. Proton conductivities of the hybrid membranes

3.4.1. Proton conductivities of the hybrid membranes at 100% RH with rising temperature

The proton conductivities of both the pristine and the hybrid Nafion membranes were characterized at 100% RH and different temperatures as shown in Fig. 9. Since the proton conducting process is thermally activated, the proton conductivities were

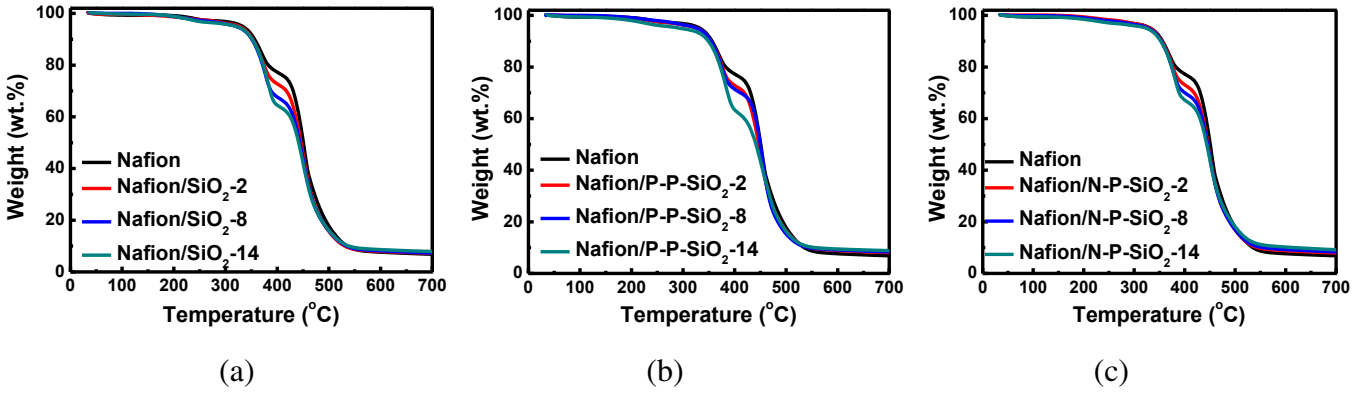

Fig. 6. TGA curves of the pristine Nafion membrane and the (a) Nafion/SiO_2, (b) Nafion/P–P–SiO_2 and (c) Nafion/N–P–SiO_2 hybrid membranes.

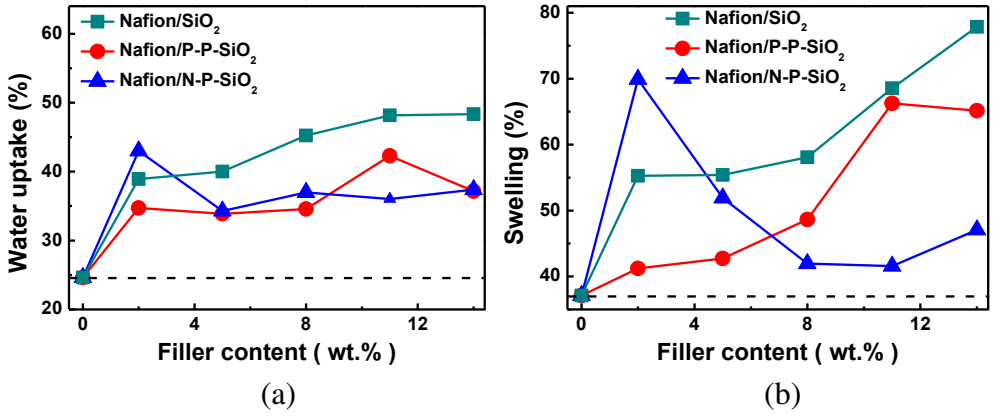

Fig. 7. The (a) water uptake properties and the (b) swelling properties of the pristine and the hybrid Nafion membranes at 25 °C.

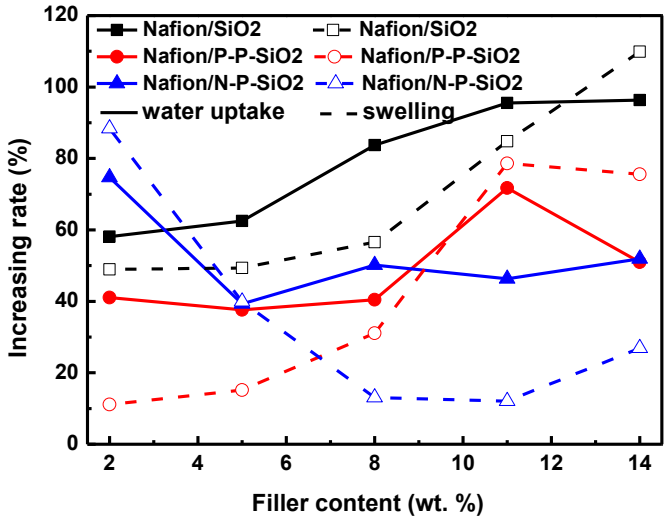

Fig. 8. The increasing rates of both the water uptake and swelling properties of the pristine and hybrid Nafion membranes at 25 °C.

enhanced with the elevating temperature for all the membranes. After the incorporation of both SiO_2 and the modified mesoporous silica submicrospheres, proton conductivities were enhanced for the hybrid membranes, while the enhancements were limited with the increase of the inorganic content attributed to the relative lower proton conductivities of the inorganic fillers than those of the organic matrix. While it should be mentioned that the proton conductivities of the Nafion/P–P–SiO_2 hybrid membranes were first increased with the inorganic content increasing from 2 wt.% to 5 wt.%, and then decreased with the further increasing content. The highest proton conductivity was 0.339 S cm^{-1} at 115 °C for the Nafion/P–P–SiO_2–5 hybrid membrane.

In this study, the content of the phosphorus element of P–P–SiO_2 has been measured by ICP. However, it should be mentioned that during the phosphorylation of epoxy groups with $POCl_3$, several side reactions could take place including the hydrolysis and the crosslinking of the phosphates [19]. As a result, not all of the phosphorus elements existed in the state of $-PO_3H_2$ groups. By ICP characterization, the weight content of the phosphorus element was 3.72 wt.%, and listed without further calculations. Herein, the approximate contents of $-PO_3H_2$ groups could be estimated as 1.2 mmol g^{-1}. It could be inferred that the IEC values of the inorganic fillers were higher than that of the Nafion membrane matrix (the IEC of the Nafion membrane is 0.852 mmol g^{-1} [32]). Thus more proton conducting groups could be introduced by P–P–SiO_2, leading to the enhanced proton conductivities of the Nafion/P–P–SiO_2 hybrid membranes with the increasing content from 2 to 5 wt.%.

With the increasing contents of inorganic fillers to 11 wt.% and 14 wt.%, the proton conductivities were reduced to nearly the same level for all the hybrid membranes. Thus, for simplicity, the proton

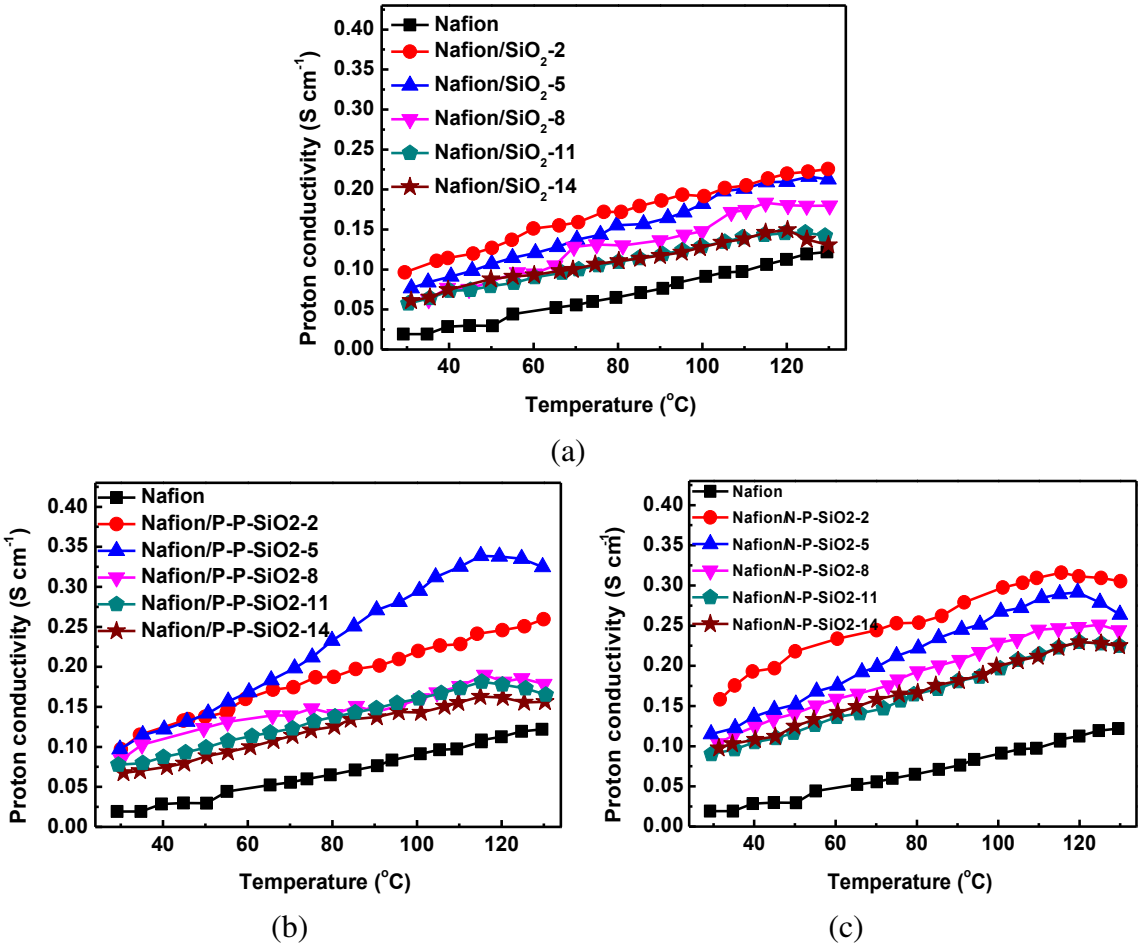

Fig. 9. The proton conductivities of the pristine Nafion membrane and the (a) Nafion/SiO_2, (b) Nafion/P–P–SiO_2 and (c) Nafion/N–P–SiO_2 hybrid membranes at 100% RH and rising temperature.

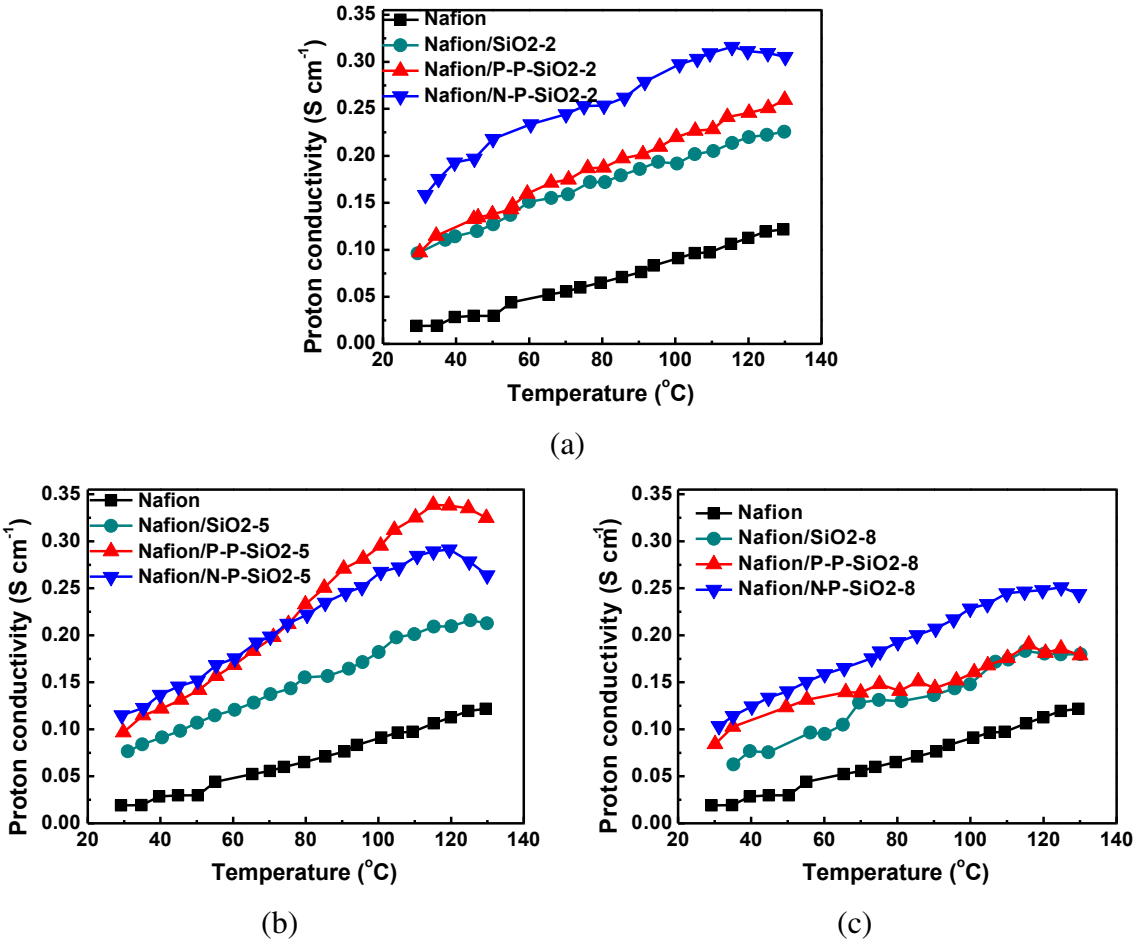

Fig. 10. The proton conductivities of the pristine and the hybrid Nafion membranes with the inorganic fillers of (a) 2 wt.%, (b) 5 wt.% and (c) 8 wt.% at 100% RH and rising temperature.

conductivities of both the pristine and the hybrid membranes were illustrated in Fig. 10, where only the hybrid membranes with the inorganic contents of 2 wt.%, 5 wt.% and 8 wt.% were illustrated.

It was clearly shown from Fig. 10 that the proton conductivities of the Nafion/SiO_2 hybrid membranes were higher than the pristine Nafion membrane, and those of the Nafion/P–P–SiO_2 hybrid membranes were even much higher. As a whole, the Nafion/N–P–SiO_2 hybrid membranes exhibited best proton conducting performance. It is well accepted that there are primarily two kinds of proton conducting mechanisms in PEMs, *i.e.* vehicle mechanism and Grotthuss mechanism [33]. On one hand, protons are transported in the form of hydronium ions (*e.g.* Zundel ions $H_5O_2^+$ and Eigen ions $H_9O_4^+$) in the proton conducting media like water environments. The excess protons are generated by the dissociation of the acidic groups in the membrane, and stabilized by the hydration shells to screen the electrostatic attractions from the conjugated bases. On the other hand, the Grotthuss mechanism is the structural diffusion of the proton defects. Proton conduction is facilitated by the continuous forming and breaking of the hydrogen bonds in the hydrogen networks arising from the solvent molecules. It is

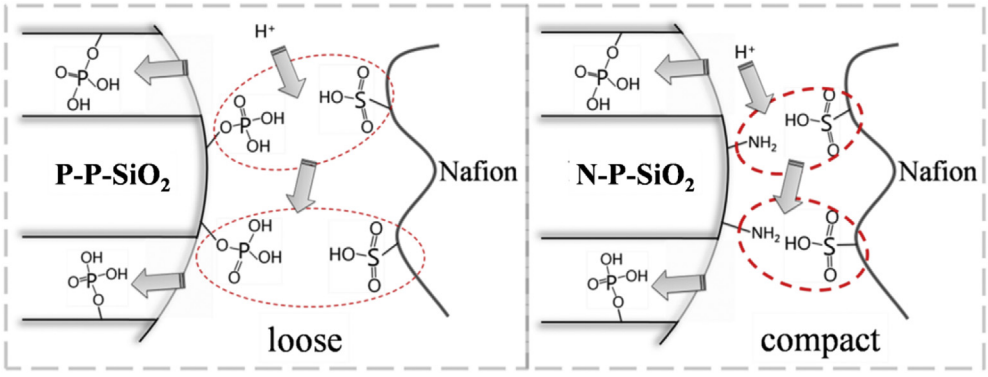

Scheme 2. Schematic depiction of the proton transport mechanisms in the hybrid membranes.

Table 2
Activation energy of proton conductivity (E_a) for the membranes.

Samples	Activation energy E_a (kJ mol^{-1})
Nafion	19.0
Nafion/SiO_2–2	8.3
Nafion/SiO_2–5	10.8
Nafion/SiO_2–8	11.4
Nafion/SiO_2–11	9.5
Nafion/SiO_2–14	8.4
Nafion/P–P–SiO_2–2	9.1
Nafion/P–P–SiO_2–5	13.3
Nafion/P–P–SiO_2–8	6.8
Nafion/P–P–SiO_2–11	8.9
Nafion/P–P–SiO_2–14	9.5
Nafion/N–P–SiO_2–2	6.6
Nafion/N–P–SiO_2–5	9.6
Nafion/N–P–SiO_2–8	9.1
Nafion/N–P–SiO_2–11	9.9
Nafion/N–P–SiO_2–14	9.2

suggested that the intramolecular charge transfer and the rearrangement of the shell water molecules occur in this process. Herein, abundant proton conducting groups should be anchored in the PEMs to generate numerous protons, meanwhile, substantial mounts of water molecules together with extensive hydrogen bond networks should exist in the PEMs to facilitate proton conduction. Proton conducting processes in the hybrid membranes were analyzed as follows and depicted in Scheme 2.

It has been discussed that the hygroscopic Si–OH groups on the silica surface and the mesopores of SiO_2, with the capacity of absorbing water by capillary forces, have increased the water content in the Nafion/SiO_2 hybrid membranes. Thus, proton conductivities were enhanced by the introduction of SiO_2 submicrospheres. For both P–P–SiO_2 and N–P–SiO_2 submicrospheres, $-PO_3H_2$ groups were anchored on the inner pore walls; and together with water molecules confined in the mesopores, proton conducting channels could be formed in the inorganic fillers, leading to fast proton conduction based on the Grotthuss mechanism. However, different kinds of proton conducting groups were anchored on the outer surface, as a result, different proton acceptor–donator interactions were fabricated especially in the organic–inorganic interface zone (depicted in Scheme 2). By introducing P–P–SiO_2 into Nafion matrix, proton conduction could be facilitated by the added proton conducting groups and the weaker proton acceptor–donator interactions between the $-PO_3H_2$ groups on the outer surface of P–P–SiO_2 and the $-SO_3H$ groups of Nafion matrix. Hence, proton conducting performances of Nafion/P–P–SiO_2 membranes were further enhanced than those of Nafion/SiO_2 membranes. More proton conducting groups could be introduced by P–P–SiO_2, thus proton conductivities were elevated with the content from 2 wt.% to 5 wt.%. In contrast, the tight complexes of the proton accepting groups ($-NH_2$ groups) and the proton donating groups ($-SO_3H$ groups) formed in the organic–inorganic interface zone of the Nafion/N–P–SiO_2 membranes were more favorable for proton conducting process. Other than restricting the

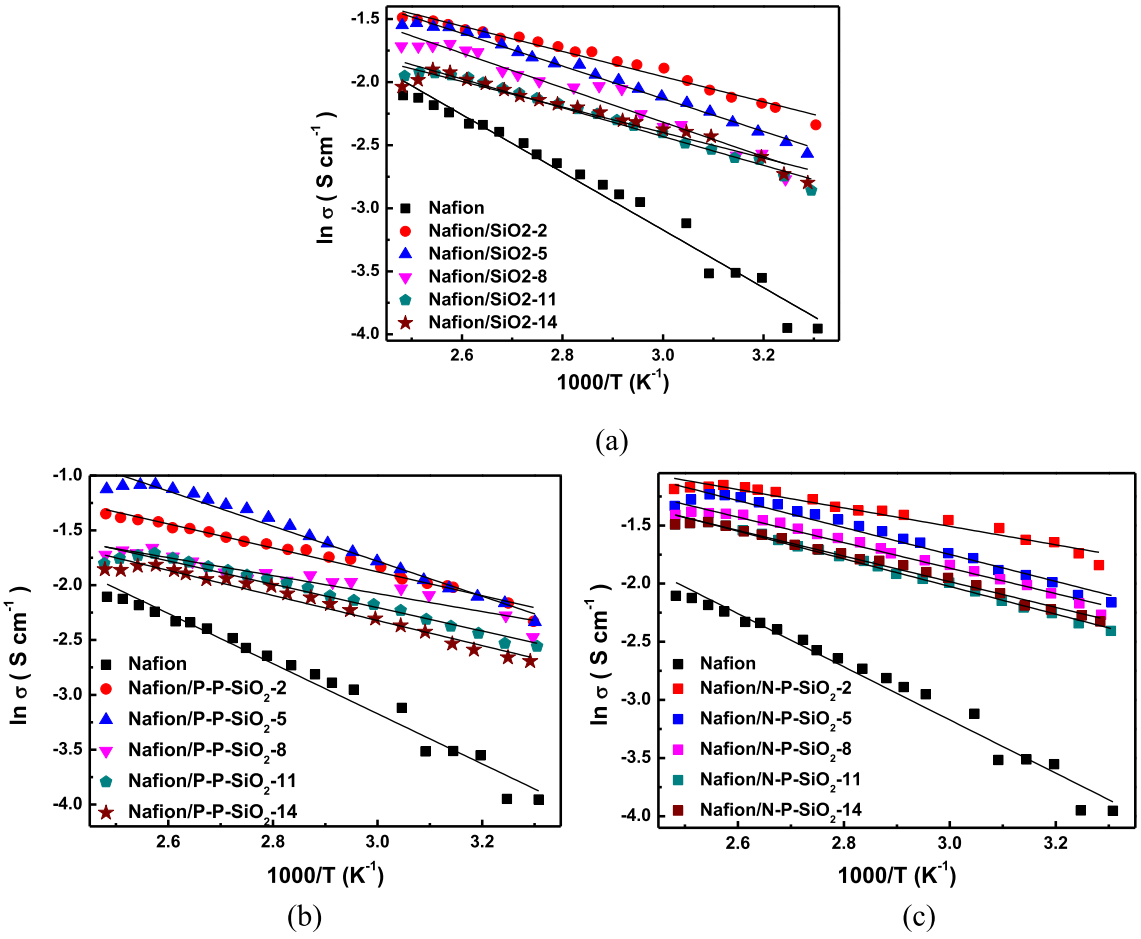

Fig. 11. Temperature-dependent proton conductivity of the pristine and hybrid Nafion membranes at 100% RH.

–SO_3H groups in the membrane matrix, more extensive hydrogen bond networks could be generated in the hybrid membranes, and proton transports could be accelerated especially along the organic–inorganic interfaces. Hereby, in general, the Nafion/N–P–SiO_2 membranes possess the best proton conducting performance at 100% RH with rising temperature. While no proton donators were introduced into the hybrid membranes with the increasing content of N–P–SiO_2, the enhancements of the proton conductivities were limited with more inorganic fillers incorporated.

The activation energy (E_a) of the proton conductivity (Table 2) for each membrane was estimated from the gradient of the fitting line by the following equation (shown in Fig. 11):

$$\sigma = \sigma_0 \exp(-E_a/KT) \quad (4)$$

It was confirmed that the activation energy for the pristine recast Nafion membrane was 19.0 kJ mol^{-1}. While the activation energy for the hybrid membranes was lower than that of the pristine Nafion membrane, suggesting the proton conducting energy barrier was lowered by incorporating the mesoporous silica submicrospheres. A plausible explanation was that additional proton conducting groups were introduced by the modified mesoporous silica, and proton conducting channels could be fabricated by both the phosphorylated mesopores and the synergistic effects between the proton conducting groups introduced by the mesoporous silica and the membrane matrix.

3.4.2. *Proton conductivities of the hybrid membranes at 80 °C and low humidities*

Proton conductivities of both the pristine and the hybrid Nafion membranes at 80 °C and low relative humidities were tested and shown in Fig. 12. It was clear that proton conductivities of all the membranes increased with the increasing relative humidities, and were enhanced for the Nafion/SiO_2 hybrid membranes compared to the pristine Nafion membrane. Proton conducting performances were further enhanced by the introduction of the functionalized mesoporous silica. However, differing from the performances at 100% RH, proton conductivities of Nafion/P–P–SiO_2 hybrid membranes were higher than those of Nafion/N–P–SiO_2 hybrid membranes at low humidities. For the proton conducting process at low humidities, abundant water molecules were needed to participate in proton conduction and fabricate hydrogen bond networks. It is accepted that the –PO_3H_2 groups are alternative candidates as proton conducting groups with great potential especially for the fuel cell working conditions at high temperature and low humidity. On the condition of lacking water, –PO_3H_2 groups could both provide protons as proton donators and stabilize excess protons as proton acceptors, and also exhibit high dielectric constant property, high water binding energy, low average zero point energy and superior thermo-oxidative stability. Thus, facilitated by –PO_3H_2 groups, extensive hydrogen bond networks could be formed by the high concentration of dissociated protons, water retention property could be enhanced and proton conduction barrier could be lowered. Hereby, proton conductivities of Nafion/P–P–SiO_2 hybrid membranes were higher than those of Nafion/N–P–SiO_2 hybrid membranes.

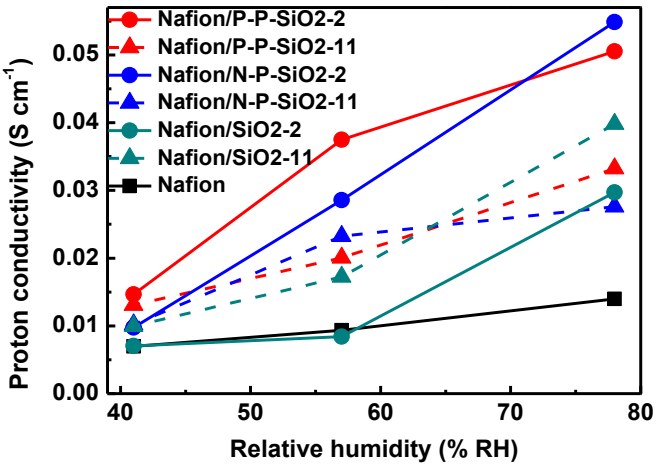

Fig. 12. The proton conductivities of the pristine and the hybrid Nafion membranes at 80 °C and low relative humidities.

4. Conclusion

Mesoporous silica submicrospheres were prepared and functionalized by different strategies: (i) –NH_2 groups were anchored on the outer surface of SiO_2, and –PO_3H_2 groups were anchored on the inner pore walls; (ii) –PO_3H_2 groups were anchored on both the outer surface and the inner pore walls of SiO_2. The functionalized SiO_2 were incorporated into Nafion matrix to fabricate hybrid proton exchange membranes. Proton conducting performances of all the hybrid membranes were enhanced than that of the pristine Nafion membrane. When utilized at 100% RH with rising temperatures, Nafion/N–P–SiO_2 membranes showed higher proton conductivities than Nafion/P–P–SiO_2 membranes; while under the conditions of 80 °C and low humidities, Nafion/P–P–SiO_2 membranes exhibited superior proton conducting performance to Nafion/N–P–SiO_2 membranes. The different behaviors could be attributed to the different chemical structures of the modified SiO_2 and the different synergistic effects between the proton conducting groups anchored on the silica surfaces and in the membrane matrix. Under the saturated humidity, the tight complexes of the proton accepting groups (–NH_2 groups) and the proton donating groups (–SO_3H groups) formed in the organic–inorganic interface zone of the Nafion/N–P–SiO_2 membranes were more beneficial for protons hopping through the extensive hydrogen bond networks along the inorganic fillers. On the contrary, abundant water molecules were needed to participate in proton conduction and construct hydrogen bond networks for the proton conducting process under low humidities, which could be assisted by the incorporated P–P–SiO_2 with larger amounts of –PO_3H_2 groups. The rational manipulation of the chemical structures of the inorganic fillers is of great significance for fabricating high-performance hybrid proton exchange membranes.

Acknowledgments

The authors gratefully acknowledge financial support from the National Science Fund for Distinguished Young Scholars (21125627), Program for New Century Excellent Talents in University (NCET-10-0623), and the Programme of Introducing Talents of Discipline to Universities (No. B06006).

References

[1] L. Vilciauskas, M.E. Tuckerman, G. Bester, S.J. Paddison, K.-D. Kreuer, Nat. Chem. 4 (2012) 461–466.
[2] S. Fujita, A. Koiwai, M. Kawasumi, S. Inagaki, Chem. Mater. 25 (2013) 1584–1591.
[3] O.F. Mohammed, D. Pines, J. Dreyer, E. Pines, E.T.J. Nibbering, Science 310 (2005) 83–86.
[4] F. Garczarek, K. Gerwert, Nature 439 (2006) 109–112.
[5] D. Cozzi, C. de Bonis, A. D'Epifanio, B. Mecheri, A.C. Tavares, S. Licoccia, J. Power Sources 248 (2014) 1127–1132.

[6] H. Zhang, C. Ma, J. Wang, X. Wang, H. Bai, J. Liu, Int. J. Hydrogen Energy 39 (2014) 974–986.
[7] H. Zhang, T. Zhang, J. Wang, F. Pei, Y. He, J. Liu, Fuel Cells 13 (2013) 1155–1165.
[8] S.Y. Han, J. Park, D. Kim, J. Power Sources 243 (2013) 850–858.
[9] D. Gupta, A. Madhukar, V. Choudhary, Int. J. Hydrogen Energy 38 (2013) 12817–12829.
[10] D.J. Kim, H.Y. Hwang, S.Y. Nam, Macromol. Res. 21 (2013) 1194–1200.
[11] J. Pan, S. Wang, M. Xiao, M. Hickner, Y. Meng, J. Membr. Sci. 443 (2013) 19–27.
[12] A.K. Mishra, S. Bose, T. Kuila, N.H. Kim, J.H. Lee, Prog. Polym. Sci. 37 (2012) 842–869.
[13] C. Laberty-Robert, K. Vallé, F. Pereira, C. Sanchez, Chem. Soc. Rev. 40 (2011) 961–1005.
[14] S.P. Jiang, J. Mater. Chem. A 2 (2014) 7637–7655.
[15] O.F. Mohammed, D. Pines, E.T.J. Nibbering, E. Pines, Angew. Chem. Int. Ed. 46 (2007) 1458–1461.
[16] D. Stoner-Ma, A.A. Jaye, P. Matousek, M. Towrie, S.R. Meech, P.J. Tonge, J. Am. Chem. Soc. 127 (2005) 2864–2865.
[17] B.J. Siwick, H.J. Bakker, J. Am. Chem. Soc. 129 (2007) 13412–13420.
[18] D. Lin, Q. Cheng, Q. Jiang, Y. Huang, Z. Yang, S. Han, Y. Zhao, S. Guo, Z. Liang, A. Dong, Nanoscale 5 (2013) 4291–4301.
[19] Y. Zhao, Z. Jiang, D. Lin, A. Dong, Z. Li, H. Wu, J. Power Sources 224 (2013) 28–36.
[20] S.-X. Zhao, L.-J. Zhang, Y.-X. Wang, J. Power Sources 233 (2013) 309–312.
[21] W.-F. Chen, Y.-C. Shen, H.-M. Hsu, P.-L. Kuo, Polym. Chem. 3 (2012) 1991–1995.
[22] J. Shi, X. Wang, Z. Jiang, Y. Liang, Y. Zhu, C. Zhang, Bioresour. Technol. 118 (2012) 359–366.
[23] Y. Zhao, Z. Jiang, L. Xiao, T. Xu, H. Wu, J. Power Sources 196 (2011) 6015–6021.
[24] C.-H. Tsai, J.L. Vivero-Escoto, I.I. Slowing, I.-J. Fang, B.G. Trewyn, V.S.-Y. Lin, Biomaterials 32 (2011) 6234–6244.
[25] B. Muriithi, D.A. Loy, J. Mater. Sci. 49 (2013) 1566–1573.
[26] K. Hooshyari, M. Javanbakht, L. Naji, M. Enhessari, J. Membr. Sci. 454 (2014) 74–81.
[27] T.-S. Chung, L.Y. Jiang, Y. Li, S. Kulprathipanja, Prog. Polym. Sci. 32 (2007) 483–507.
[28] T.T. Moore, W.J. Koros, J. Mol. Struct. 739 (2005) 87–98.
[29] Y. Li, G. He, S. Wang, S. Yu, F. Pan, H. Wu, Z. Jiang, J. Mater. Chem. A 1 (2013) 10058–10077.
[30] J. Wang, X. Yue, Z. Zhang, Z. Yang, Y. Li, H. Zhang, X. Yang, H. Wu, Z. Jiang, Adv. Funct. Mater. 22 (2012) 4539–4546.
[31] A.G. Kannan, N.R. Choudhury, N.K. Dutta, J. Membr. Sci. 333 (2009) 50–58.
[32] Z. Jiang, X. Zheng, H. Wu, J. Wang, Y. Wang, J. Power Sources 180 (2008) 143–153.
[33] T.J. Peckham, S. Holdcroft, Adv. Mater. 22 (2010) 4667–4690.